J MATER SCI 41 (2006) 2939–2951

Structure, properties and fracture of friction stir welds in a high-temperature Al-8.5Fe-1.3V–1.7Si alloy (AA-8009)

W. A. BAESLACK III*
College of Engineering The Ohio State University, Columbus, OH 43210, USA
E-mail: baeslack.1@osu.edu

K. V. JATA
Materials and Manufacturing Directorate, Air Force Research Laboratory, Wright-Patterson AFB, OH, 45431, USA

T. J. LIENERT
MST Division, Los Alamos National Laboratory, Los Alamos, NM 87545, USA

Published online: 21 April 2006

Friction stir welds produced in a rapidly-solidified, powder metallurgy Al-8.5Fe-1.3 V-1.7 Si (wt.%) alloy were characterized in order to investigate the effects of deformation during welding on the weld zone microstructure, hardness, tensile properties, and fracture behavior. A weld produced using a tool rotational speed of 1200 rpm and a traversing rate of 4.3 mm/s exhibited a repetitive pattern of dispersoid-depleted bands that were attributed to the intense deformation that occurred in the vicinity of the tool. The significant softening associated with these regions, and the presence of occasional, irregularly-shaped voids near the boundary between the base metal and the weld zone on the advancing side of the weld, promoted a weld tensile strength of 60–70% of the base metal. The application of a lower tool rotational speed of 428 rpm and a lower traversing rate of 1.9 mm/s promoted fewer bands and a more uniform dispersoid distribution throughout the weld zone, and an absence of defects along the weld zone/base metal interface. Tensile strength of these welds approached 90% of the base metal. Fracture of the transverse-weld oriented tensile specimens for both weld types consistently occurred near the boundary between the weld zone and the base metal on the advancing side of the weld zone, with tensile specimen ductilities appreciably lower than that of the base metal.

1. Introduction

1.1. Friction stir welding

Friction stir welding (FSW) is a relatively new joining process in which a rotating, non-consumable pin is advanced between two contacting metal plates. The threaded pin is coaxially attached to a cylindrical tool shoulder that rotates at several hundred revolutions per minute. The welding process is initiated by plunging the rotating pin into the workpieces at the joint interface until the tool shoulder impinges the top surface of the workpieces, and following a short dwell time, translating it along the length of the joint. The localized frictional heating and thermo-mechanical deformation experienced at the weld interface promotes the production of a high-integrity, solid-state weld. At the end of the joint, the tool is stopped and withdrawn from the workpiece. The FSW process has been widely applied for the welding of aluminum alloys, as it offers many advantages over the conventional fusion welding of these alloys, in particular the elimination of solidification and liquation cracking, and porosity. In contrast to the relatively coarse grains that typically characterize fusion welds, plastic deformation and dynamic recrystallization that occur during the FSW process promote formation of a fine-grained weld zone microstructure.

*Author to whom all correspondence should be addressed.
0022-2461
DOI: 10.1007/s10853-006-5089-y

The FSW process exhibits asymmetry due the combination of rotation and translation of the tool. A nomenclature has been developed to describe the features of the process. The advancing side of the weld is defined as the side where the tool rotation direction is parallel to the tool translation direction. Conversely, the retreating side of the weld is identified as the side where the tool rotation and translation vectors are anti-parallel.

Solid-state metal flow during FSW is extremely intense (i.e., high strains and strain rates) and nonuniform, which can result in the formation of heterogeneous weld zone microstructures. Lienert *et al*. [1] observed bands in the weld zone of friction stir welds in 6061-T651 aluminum, and attributed them to regions that interacted most closely with the pin, and that experienced the greatest strains and strain rates as well as the highest temperatures. They observed a decreased intermetallic particle size in these bands relative to the base metal and bulk weld zone, and attributed this to their crushing and/or partial dissolution.

Extensive studies by Murr and co-workers [2–6], on both similar-alloy welds, and dissimilar-alloy welds between aluminum and copper and between different aluminum alloys, have shown the extensive plastic deformation during FSW to create complex vortex and swirl-like structures, especially near the weld zone/base metal interface. In dissimilar aluminum alloy welds they observed striations and patterns of compositional difference that corresponded to the spacing of the pin threads. They further noted that the formation of these patterns is influenced by the pin geometry and rotational speed.

Several investigators have utilized experimental tracer techniques [7–12] and mathematical modeling [13–17] to investigate the nature of plastic deformation and metal flow during FSW. Pioneering work by Colligan [7] utilized steel shot markers placed at different plate depths and lateral distances from the weld centerline in an Al alloy. The position of the steel shot was recorded after welding using radiography. The markers initially placed near the top of the plate were lifted as they approached the tool and were deposited in a chaotic and random fashion behind the tool. Some of the material originally near the top surface was subsequently carried downward by the threads on the pin. Markers located originally near the mid-thickness of the plate were also lifted in front of the tool, and those positioned in the path of the pin were transported around the retreating side of the tool. Markers positioned near the bottom of the plate passed under the pin without lifting.

Seminal efforts by Reynolds and coworkers [8–10] using markers in the form of plugs of dissimilar Al alloys with different etching response revealed that material is carried forward on the advancing side of the pin and backward around the retreating side. In addition, the stir zone took on a more rounded shape with increasing diameter of the pin with the maximum stir zone width occurring near the plate mid-thickness. The largest pin diameter produced a large bulge on the advancing side of the stir zone.

A thin sheet of copper placed along the weld joint was employed by Guerra *et al*. [11] as a marker. They stated that the metal enters a relatively narrow "rotational zone" that rotates and advances with the pin. Material within this region is transported vertically in a helical motion, initially upward, and then, under the influence of the pin threads, in a downward spiral toward the bottom of the weld, and finally upward again. Material in the rotational zone ultimately "sloughs off" in arc-shaped features that produce the intercalated weld "stir zone" microstructures.

London *et al*. [12] utilized composite markers of Al-SiC and Al-W placed near the plate midplane on both the advancing and retreating sides. They also showed that markers are lifted in front of the tool and subsequently carried downward by the threads. In addition, markers initially on the advancing side were distributed over a wider region.

Computer modeling using a computational fluid dynamics (CFD) approach was employed by Bendszak *et al*. [13] to study material flow during FSW. They reported three distinct flow regimes that occur at different depths: (1) a region of rotation just under the shoulder where flow occurs in the direction of tool rotation; (2) a region near the base of the pin where material is extruded past the pin; and (3) a transition region between regions 1 and 2 where flow is chaotic. Of particular interest in the transition region is the report of an unstable region where flow reversal occurs at a location where the rotational and translational velocities of the tool are equal in magnitude and opposite in direction.

Deng and coworkers [14, 15] developed a solid-mechanics model to analyze flow during FSW. Their model was able to closely reproduce the experimental marker studies of Reynolds and coworkers. They also suggested that material tended to pass mainly around the retreating side of the pin.

The flow of material around the retreating side of the pin was corroborated with a CFD model advanced by Seidel and Reynolds [16, 17]. Their results indicated that streamlines split in front of the pin on the advancing side. Material within the pin diameter was transported around the retreating side of the pin in the direction of rotation following arced paths shaped like concentric horseshoes (or the Greek letter Ω). The streamlines subsequently rejoined behind the pin on the advancing side. The pattern of streamlines around the pin was determined to occur

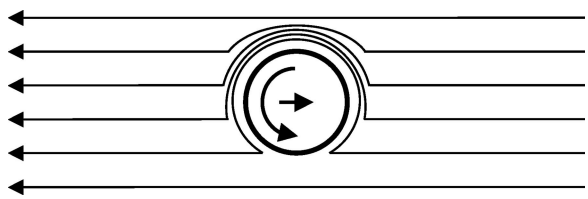

Figure 1 Pattern of flowlines around FSW pin. The tool moves to the right and rotates in a CCW direction when viewed from above. The retreating side is at the top and the advancing side is at the bottom. Adapted from [16, 17].

as shown in Fig. 1. The material that passed around the retreating side of the pin was deposited behind the pin in the same lateral position relative to the jointline as it originated. Consequently, material originally located far on the advancing side (but within the pin diameter), was transported a greater distance relative to the material initially located closer to the retreating side and thus experienced greater strains. Since the same material travels a greater distance in the same time period (~1 revolution of the pin), it also was subjected to greater strain rates. These authors also suggested that excessive rotational speeds (RPMs) may allow some material to flow around the advancing side and that this condition may lead to the formation of lack of bonding defects.

1.2. Al-Fe-V-Si alloys

Al-Fe-V-Si alloys represent a unique class of aluminum alloys for high performance applications at temperatures up to 400°C, well above the service temperatures of conventional elevated-temperature aluminum alloys such as 2219 [18, 19]. The hypereutectic Al-Fe compositions (8.5–12 wt.% Fe) of these alloys require their production using rapid solidification/powder metallurgy (RS/PM). Through RS/PM processing, a unique microstructure can be achieved that consists of a high volume fraction of nearly-spherical, submicron $Al_{13}(Fe,V)_3Si$ dispersoids in an extremely fine-grained alpha aluminum matrix. The low interfacial energy between these dispersoids and the matrix, and the low solid-state diffusivity of transition elements in alpha aluminum, minimize dispersoid coarsening, thereby enhancing particle stability and useful mechanical properties to temperatures approaching 400°C.

1.3. Friction welding of Al-Fe-V-Si alloys

The joining of two Al-Fe-V-Si alloys, Fe-8.5Al-1.3V-1.7Si (AA-8009) and Fe-11.7Fe-1.2V-2.4Si (FVS1212), as well as an 8009/SiC/11 p metal matrix composite has been successfully accomplished using both the inertia-friction and linear-friction welding processes [20–24]. These processes combine frictional heat generated at the workpiece faying surfaces through rotational or linear motion with a high axial force to produce a metallic bond. The solid-state nature of the processes eliminates the potential for hydrogen-induced porosity that severely limits the fusion weldability of these alloys. Furthermore, the rapid thermal cycle experienced, and the expulsion of surface contaminants and severely heat-and-deformation-affected metal present at the weld interface during the final forging stage of the processes, promote final coalescence between nearly unaffected base metals, thereby promoting high joint strengths approaching that of the base metal.

Detailed characterization of inertia-friction and linear-friction welds in Al-Fe-V-Si alloys and metal-matrix composites using light, scanning-electron and transmission-electron microscopy has revealed that intense, high-temperature plastic deformation at the center of the weld zone effectively homogenizes the base metal microstructure and does not promote significant dispersoid coarsening or dispersoid fracture processes [20–24]. However, inertia-friction welds produced at low axial force exhibited dispersoid-lean, coarse-grained regions at the weld outer periphery with hardnesses appreciably below that of the bulk weld zone. Correspondingly, regions that exhibited a higher than average population density of dispersoids were also often observed adjacent to the lean regions.

The overall objective of the present study was to determine the feasibility of producing high-integrity friction stir welds in rapidly-solidified Al-8Fe-1.3V-1.7Si. More specifically, this work examined the influence of welding parameters on weld integrity and microstructure, and in particular the effect of the intense, nonuniform deformation known to occur during FSW on the distribution of dispersoids in the weld zone. These weld microstructural characteristics were subsequently correlated with weld zone hardness, tensile strength and ductility, and fracture behavior.

2. Experimental

Friction stir butt welds were produced at Edison Welding Institute between 76.2 × 203 × 6.3 mm plates of extruded AA-8009 using a tool rotational speed of 1200 revolutions per minute and traversing rate of 4.3 mm/s (designated as Weld 1), and a lower tool rotational speed of 428 revolutions per minute and a lower traversing rate of 1.9 mm/s (designated as Weld 2). The plates were held in compression and were rigidly clamped to the machine bed during welding. Both welds were produced with the welding direction parallel to the plate extrusion direction. The FSW tool was fabricated from H-13 tool steel with a 19.1 mm shoulder diameter and a 6.4 mm pin diameter.

Subsequent to FSW, the welds were sectioned into specimens for metallographic examination using light and scanning-electron microscopy, hardness and tensile testing. Three sections from each weld, including a plan view at 1/2 depth through the specimen thickness, a transverse section perpendicular to the weld traversing direction, and a longitudinal section along the center of the weld zone, were mounted in conductive epoxy, rough ground on SiC to 600 grit, and final polished using colloidal silica. As-polished specimens were examined in a scanning-electron microscope using the backscattered-electron (BE) imaging mode. Metallographic specimens were subsequently etched using Keller's etch and examined using conventional light microscopy. Following metallographic analysis, DPH hardness testing was performed on each specimen using a load of 150 g.

Three flat, transverse-weld oriented tensile specimens were extracted from each weld in accordance with ASTM Standard E8 (gage section of 35 mm in length, 12.2 mm in width) and tensile tested at room temperature at a strain rate of 1.27 mm/min. Two base metal specimens oriented

parallel to the plate extrusion direction were also tensile tested.

3. Experimental results

3.1. Microstructure analysis

The AA-8009 base metal microstructure has been described previously [20–24] and exhibited fine $Al_{13}(Fe,V)_3Si$ dispersoids ranging from about 50 to 250 nm in diameter. These dispersoids were located both within and at the boundaries of fine, nearly-equiaxed alpha aluminum grains ranging from about 0.5 to 1.0 microns in diameter. Light micrographs in Fig. 2a and b show a plan view of the base metal microstructure at the center of the plate thickness, and a transverse section oriented perpendicular to the extrusion direction, respectively. Contrast

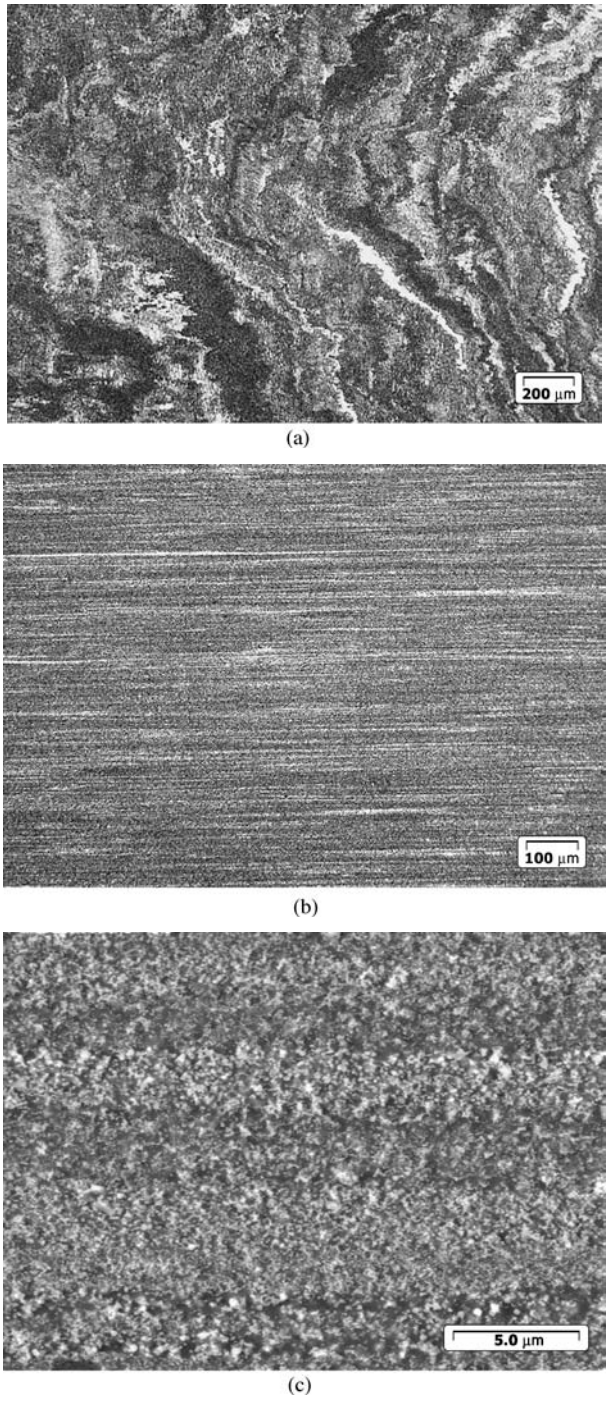

Figure 2 Light (a, b) and SEM/BSE (c) micrographs of AA-8009 base metal: (a) plan section at center of plate thickness, the extrusion direction is vertical; (b, c) transverse section perpendicular to extrusion direction.

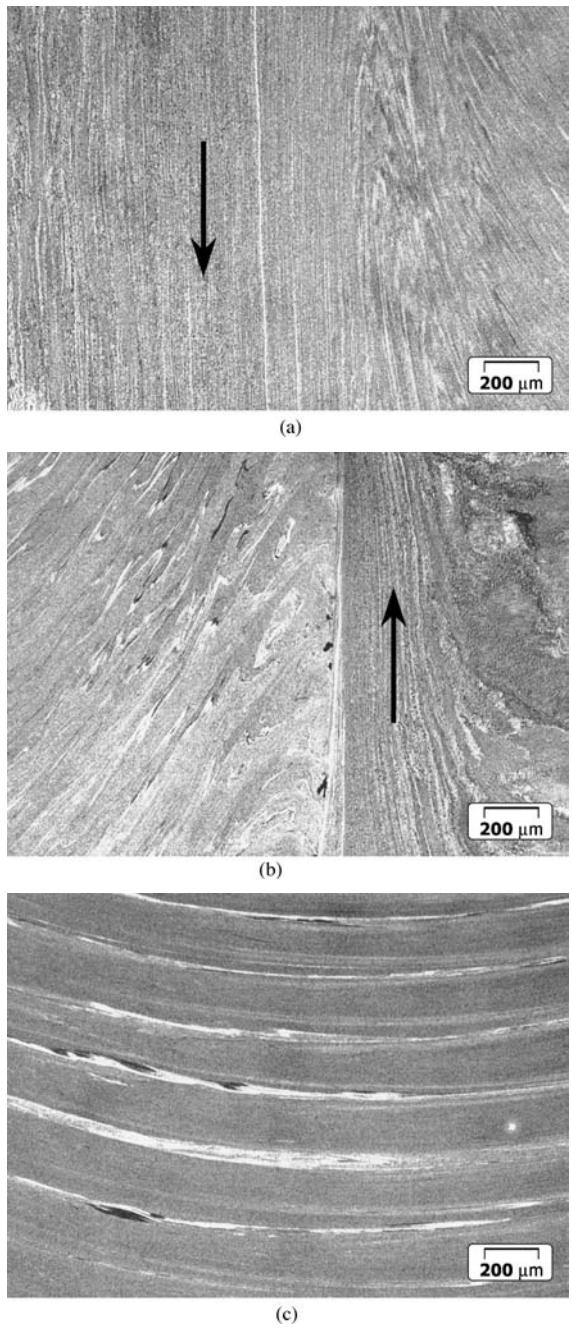

Figure 3 Light micrographs of plan section at the center of the plate thickness through FSW- 1 produced in AA-8009 at a tool rotational speed of 1200 rpm and a traversing rate of 4.3 mm/s: (a) boundary between transition zone (left side) and stir zone on the retreating side of weld (arrow indicates backward flow of material in transition zone); (b) boundary between transition zone (right side) and the stir zone on the advancing side of the weld (arrow indicates forward flow of material in transition zone); (c) center of weld stir zone. The tool rotation direction in this figure was counter-clockwise, and the tool traverse direction was upward.

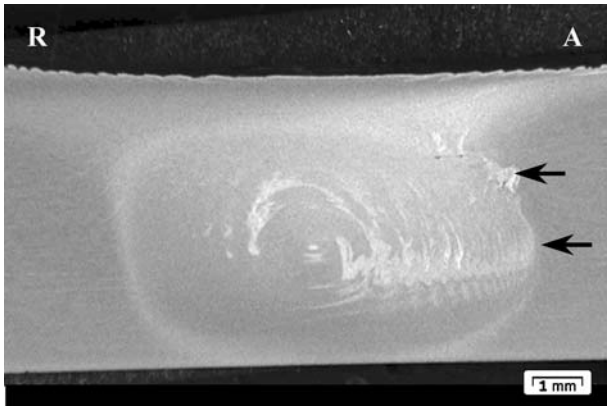

Figure 4 Light micrograph of transverse section through FSW-1 produced in AA-8009 at tool rotational speed of 1200 rpm and a traversing rate of 4.3 mm/s. Advancing side of the weld is on the right side micrograph. Upper arrow indicates location of defects, and lower arrow indicates nugget bulge.

differences resulted from local variations in the dispersoid size and population density. The SEM micrograph in Fig. 2c further reveals the variations in dispersoid size and density within the textured base metal microstructure.

Figs 3a–c illustrate a plan view of the weld zone at the center of the plate thickness for Weld 1 (produced using a tool rotational speed of 1200 rpm and a traversing rate of 4.3 mm/s). The retreating side of the weld zone shown in Fig. 3a contained a wide transition zone in which a gradual realignment of the base metal microstructure (Fig. 2a) occurred to a direction parallel to the rotation direction at the edge of the weld. Since the rotation velocity at the periphery of the pin is much greater than the translation velocity, the material in the transition zone is aligned and elongated in the tool rotation direction (which on the retreating side of the weld is anti-parallel to the translation direction). The arrow in Fig. 3a indicates backward flow of the transition zone material in accord with References [8–10]. In addition, the material in the transition zone also appears to have narrowed in the lateral direction. Although the plastic flow in this region deformed the base metal microstructure, it was not sufficient to completely homogenize the original microstructure.

At the boundary between the base metal and the weld zone on the advancing side of the weld (Fig. 3b), the transition zone was appreciably narrower than on the retreating side of the weld, At the boundary between the transition zone and "stir zone," through which the pin and surrounding rotational zone traversed, the reoriented and deformed base metal microstructure abruptly changed at a nearly discrete interface to a curvilinear orientation that continued across much of the stir zone. Evidence of fine, irregularly shaped voids could be observed at this interface. The arrow in Fig. 3b indicates the forward flow of material in the transition region on the advancing side of this weld as described in References [8–10].

Nearer to the center of the weld, the microstructure was comprised of distinct bands of alternating dark-contrast and light-contrast regions that followed a curvilinear contour (Fig. 3c). Occasional regions of black-contrast were observed adjacent and parallel to the light-contrast bands. The spacing of each light-contrast band corresponded closely to the distance of tool advance per revolution.

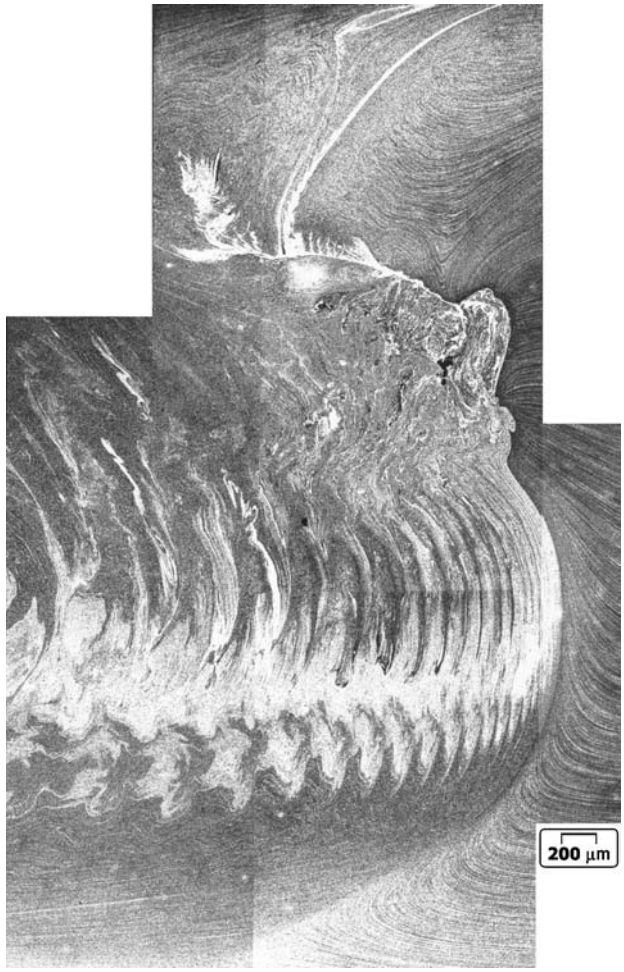

Figure 5 Light micrograph of transverse section through FSW-1 produced in AA-8009 at a tool rotational speed of 1200 rpm and a traversing rate of 4.3 mm/s showing advancing side boundary between weld stir zone and transition zone (right-side).

Figs 4 and 5 show light micrographs of a transverse section through Weld 1. Note the asymmetry of the stir zone of this weld and the bulge on the advancing side (right side of Fig. 4) of the stir zone. Consistent with the plan view of this weld, the advancing side of the weld exhibited a distinct boundary between the deformed and reoriented base metal microstructure in the transition zone and the banded microstructure in the stir zone. As indicated above, the transition zone on the retreating side of the weld was appreciably larger than on the advancing side. Furthermore, the banding in the stir zone appeared to be limited mainly to the advancing side of the weld (right side of Fig. 4). A series of bands of alternating light and dark contrast extend from the center of the stir zone to the bulge. A narrow region of light contrast can also be seen curving from the upper advancing side along the interface between the transition zone and stir zone in Figs 4 and 5. Additionally, feathery wisps of light contrast were

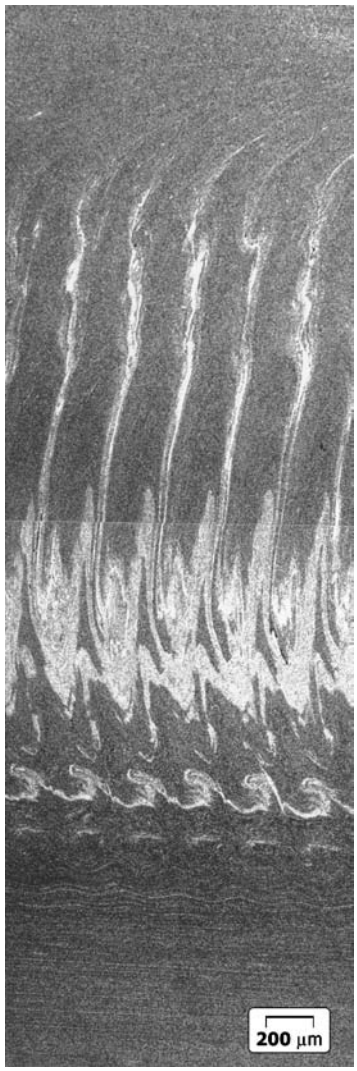

Figure 6 Light micrograph of longitudinal section through FSW-1 produced in AA-8009 using at a tool rotational speed of 1200 rpm and a traversing rate of 4.3 mm/s. The tool traverse direction is from left to right.

observed branching from this thin interface (see Fig. 5). Evidence of small voids could be observed near the interface on the advancing side of the weld, in a location consistent with that observed in the plan view of this weld.

Fig. 6 shows a longitudinal section through the Weld 1 centerline, and reveals the distinct, repetitive banding that occurred throughout about two-thirds of the weld thickness. Again, the spacing of each light-contrast band corresponded closely to the distance of tool advance per revolution. The presence of banding in the center of the weld together with the absence of banding near the top and bottom of the weld appears consistent with the different modes of deformation in the three regions described in the model by Bendszak [13].

SEM analysis of the banded regions in Weld 1 revealed a significant difference in dispersoid density between the light and dark-contrast regions observed with light microscopy (note that contrasts observed in light microscopy and SEM are reversed). As shown in Figs 7a and b, light-contrast regions in Fig. 5 at the weld interface on the weld advancing side were nearly dispersoid free, while dark-contrast bands in Fig. 5 were dispersoid rich relative to the surrounding regions (Figs 7c and d). Voids could also be observed in Fig. 7a. Note that evidence of a true heat-affected zone (HAZ) was not apparent using light microscopy or SEM analysis, which was consistent with the high-temperature stability of the base metal.

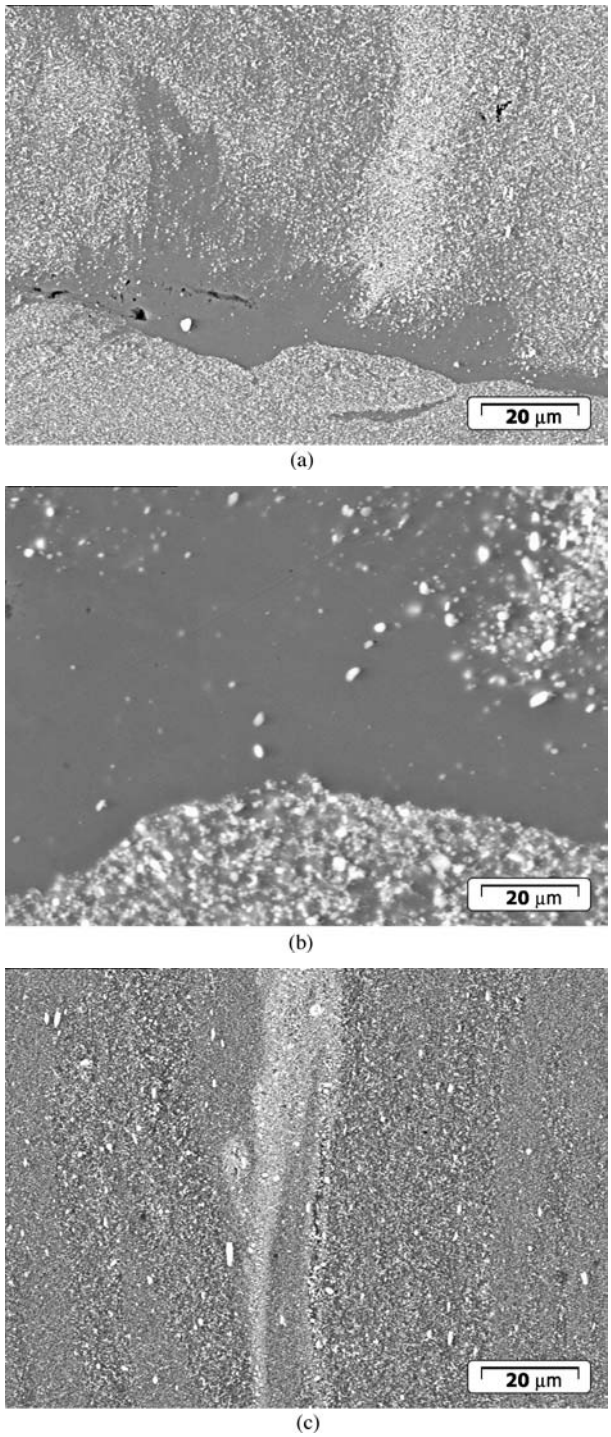

Figure 7 SEM/BSE micrographs of weld stir zone in transverse section through FSW produced in AA-8009 at a tool rotational speed of 1200 rpm and a traversing rate of 4.3 mm/s. (*Continued on next page*.)

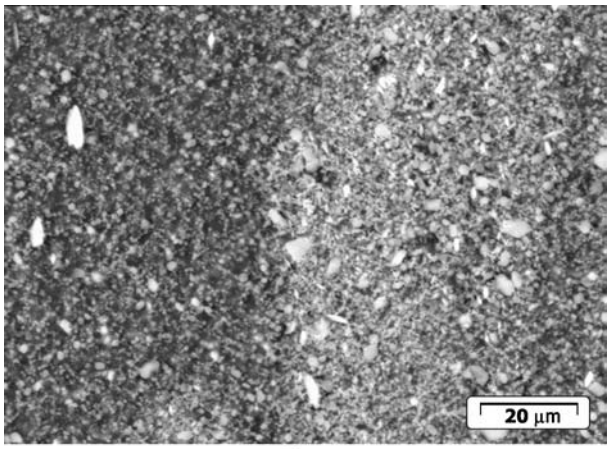

(d)

Figure 7 Continued.

Fig. 8 shows a plan section at the center of the plate thickness through Weld 2 (produced at a tool rotational speed of 428 rpm and a traversing rate of 1.9 mm/s) on both the retreating (a) and advancing (b) sides of the weld. The microstructural change from the unaffected base metal to the transition zone, which involved the reorientation and texturing of the base metal microstructure in a direction parallel to the weld traverse direction, was very gradual on the retreating side of the weld, and a distinct boundary between the transition zone and the stir zone, in which the base metal microstructure was effectively homogenized, was not apparent. Relative to Weld 1, microstructural change on the advancing side of Weld 2 from the unaffected base metal, across the transition zone, and into the stir zone was more gradual, although a distinct boundary was clearly apparent (left side of Fig. 8b). In contrast to Weld 1, voids were not observed at this boundary.

Figs 9a and b show transverse cross-sections through Weld 2. Although evidence of microstructural banding in the stir zone could be observed on the lower advancing side of the weld (left side of Fig. 9a), the extent was appreciably less than that observed in the weld produced at higher tool speed and traversing rate. Consistent with the plan view shown in Fig. 8, the transverse section clearly shows that this weld exhibited an appreciably more homogenous microstructure throughout the weld stir zone. Examination of the banded regions using SEM revealed lower dispersoid densities in the light-contrast regions, but an absence of the dispersoid-free regions observed in Weld 1. Note that this weld did exhibit a small unbonded region at the weld centerline on the bottom surface due to inadequate pin length.

3.2. Hardness and tensile properties

DPH hardness evaluation of the base metal and weld zone microstructures showed regions in which the base metal microstructure was retained and homogenized (e.g., location #7 in Fig. 9b for Weld 2) to exhibit hardnesses

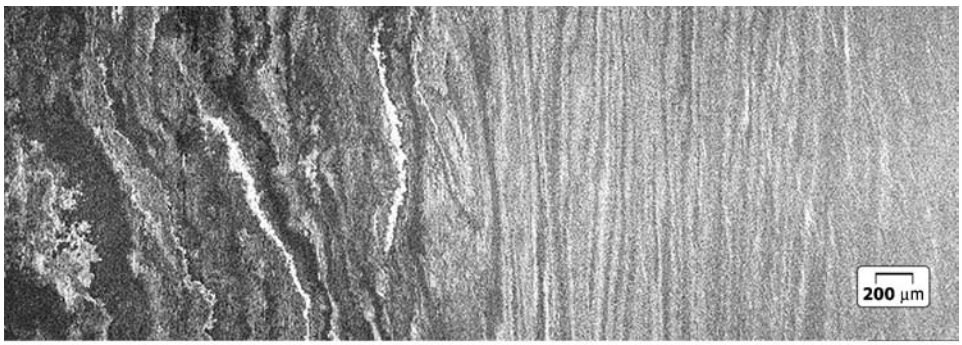

(a)

(b)

Figure 8 Light micrographs of plan section at the center of the plate thickness through FSW produced in AA-8009 at a tool rotational speed of 428 rpm and a traversing rate of 1.9 mm/s: (a) transition from unaffected base metal (left side) through transition zone and into stir zone on the retreating side of the weld; (b) transition from unaffected base metal (right side) through transition zone and into stir zone on the advancing side of the weld. The tool traverse direction in this figure was upward.

only slightly below that of the unaffected base metal (DPH 115–120 versus DPH 125–130). However, banded regions in this weld that exhibited light contrast in light microscopy and a dispersoid density below that of the base metal showed a lower hardness range of about DPH 100–110. The light-contrast, nearly dispersoid-free regions observed at the base metal/weld zone boundary in Weld 1 were very soft, as low as DPH 54 (Fig. 10).

As shown in Table I, the joint efficiency (ratio of weld tensile strength/base metal tensile strength) for Weld 1 was appreciably lower than that for Weld 2. Specimen-to-specimen variations in tensile strength and ductility were also much greater for Weld 1. Interestingly, improved microstructural homogenization of Weld 2 did not appear to enhance the tensile ductility, which was comparable for both welding conditions and appreciably lower than that of the base metal. These low ductilities can be attributed to strain localization effects in the softer weld microstructure regions (banded and others) near the stir zone/transition zone boundary on the advancing side of the weld, and possibly the presence of defects in this region in the case of Weld 1.

3.3. Fracture analysis

Base metal tensile specimens exhibited a macroscopically flat fracture surface and appreciable reduction-in-area (44%). SEM analysis of the fracture surface (Fig. 11a) showed flat regions of dimpled, ductile-appearing fracture separated by occasional tear ridges. Analysis at increased magnification (Fig. 11b) revealed microvoids that had nucleated at the interface between the soft alpha-aluminum matrix and the hard dispersoid particles. Occasional fine cracks oriented parallel to the rolling direction were also observed.

Welded specimens exhibited macroscopically irregular fracture surface topographies, with the fracture path located at or near to the boundary between the weld zone and the base metal on the advancing side of the weld. Fracture surfaces near the weld top surface visually appeared dull and gray, similar to that of the base metal. SEM analysis of this surface revealed similar evidence of microvoids and tear ridges (Figs 12a and b). However, fracture at the plate center, that typically occurred along a relatively flat surface, occasionally exhibited a shiny visual appearance. This surface appeared to be associated with the interface between the weld stir zone and the transition zone or base metal on the advancing side of the weld. Fig. 13a is an SEM micrograph of such a flat, shiny region at the center of the tensile specimen for Weld 1. Analysis at high magnification (Fig. 13b) revealed a smooth, almost featureless surface suggesting poor bonding, evidently due to the advancing side defects discussed previously.

Tensile specimen fracture surfaces for Weld 2 were relatively flat, visually gray, and exhibited no evidence of the shiny, flat regions observed in the Weld 1 specimens. As shown in Fig. 14, even regions that appeared relatively featureless at low magnification, and that were associated with the base metal/weld zone boundary on the advancing side of this weld, did indeed exhibit evidence of deformation and fracture at high magnification.

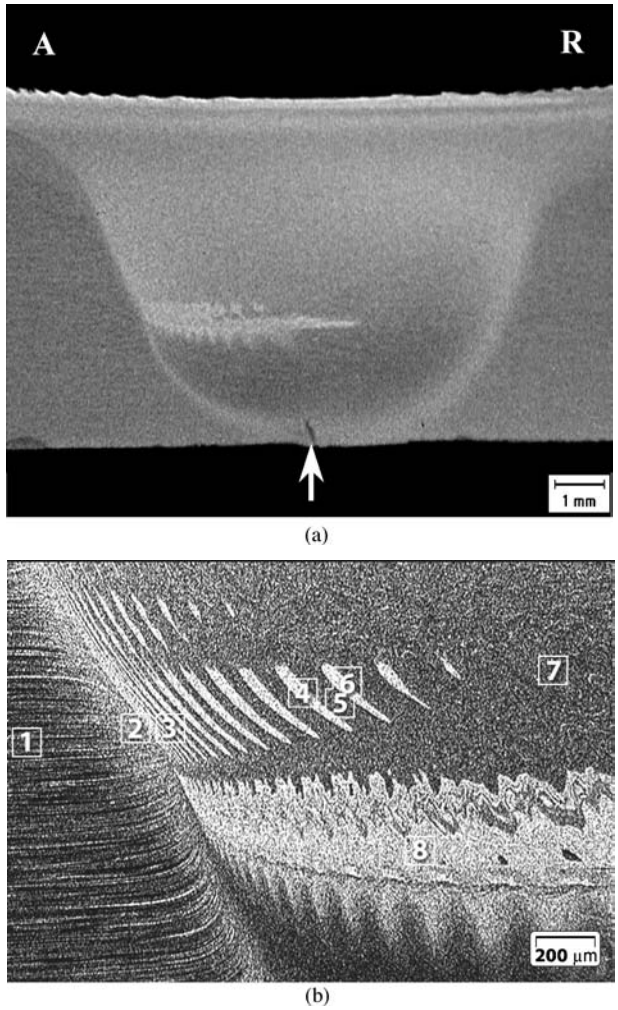

Figure 9 Light micrographs of transverse section through FSW produced in AA-8009 at a tool rotational speed of 428 rpm and a traversing rate of 1.9 mm/s. Advancing side of the weld is on the left side of the micrograph. Arrow in (a) indicates unbonded region due to insufficient pin length. DPH hardnesses associated with numbered locations in (b) are: #1—DPH 124; #2—DPH 120; #3—DPH 108; #4—DPH 109; #5—DPH 114; #6—103; #7—DPH 118; #8—DPH 102.

3.4. Discussion

This study has demonstrated that the intense (i.e. high strain and strain rate), nonuniform deformation experienced during the FSW of AA-8009 can result in the formation of a diversity of microstructures across the weld zone. In transition zones between the unaffected base metal and the stir zone, the flow of material between the base metal and the rotational zone that surrounds the moving tool deformed and further textured the base metal microstructure. In this region, the original base metal texture, which was characterized by regions of different dispersoid size and population density, was not fully homogenized. In the stir zone, intense deformation associated with FSW promoted the formation of alternating dispersoid-lean and dispersoid-rich bands in the form of distinct, repetitive

TABLE I Tensile properties of friction stir welds in Al-8009*

Specimen	Tool RPM	Travel rate (mm/s)	Yield strength (Mpa)	Ultimate tensile strength (Mpa)	Elong. (%)	RA (%)	Joint efficiency (%)
BM-1	–	–	369	440	23.9	41.8	–
BM-2	–	–	362	439	27.7	45.8	–
Weld 1-1	1200	4.3	321	338	2.4	7.2	77
Weld 1-2	1200	4.3	300	306	3.1	3.1	77
Weld 2-1	428	1.9	347	392	2.2	8.8	89
Weld 2-2	428	1.9	328	381	2.0	7.6	87
Weld 2-3	428	1.9	359	395	2.1	13.1	90

*Fracture of all welded specimens occurred near the boundary between the weld zone and the unaffected base metal

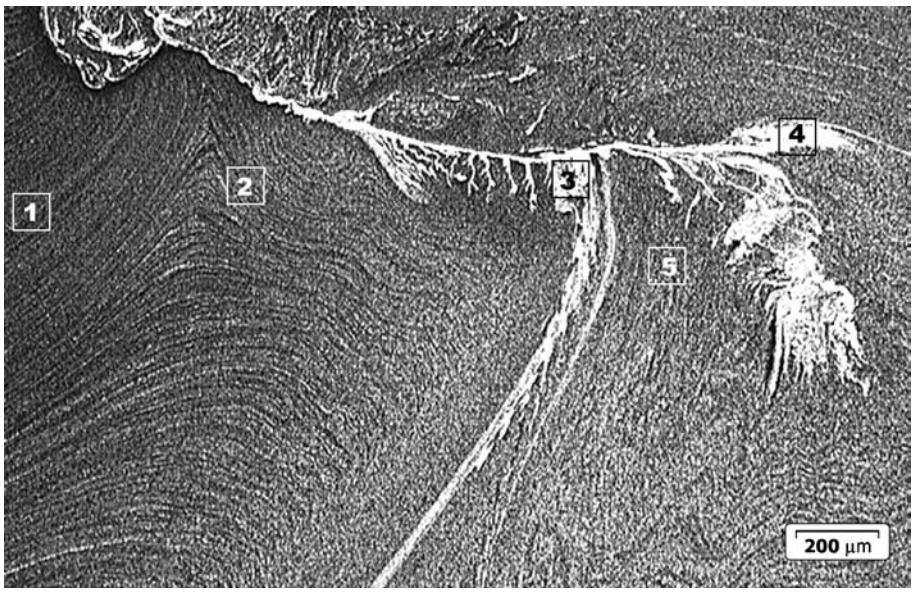

Figure 10 Light micrographs of transverse section (advancing side) through FSW produced in AA-8009 at a tool rotational speed of 1200 rpm and a traversing rate of 4.3 mm/s. DPH hardnesses associated with numbered locations are: #1—DPH 125; #2—DPH 131; #3—DPH 77; #4—DPH 54; #5—DPH 103; #6—DPH 105.

patterns especially in Weld 1, which was produced at the higher tool rotating speed and traversing rate. Outside the banded regions of the stir zone, the base metal microstructure was effectively homogenized. Although these banded regions appeared relatively simple in the plan view shown in Figs 2c, 4 and 5 reveal the highly complex geometries of these dispersoid-lean bands through the weld thickness, and their remarkably similar geometries along the weld length.

Consistent with previous observations [20, 24], the bands apparently formed in regions of highest strain and strain rate during FSW (and other friction welding processes). The bands may have formed due to some type of shear banding, possibly adiabatic shear banding [25]. There is likely a critical level of strain and/or strain rate above which the banding occurs. Consequently, this alloy may be useful for studying the relation between process parameters and local strains and strain rates during FSW. It is important to note that the critical strain/strain rate level is not currently known and that more work would be needed to determine the critical level under the stress state imposed during FSW before these studies can be undertaken.

Strain rates during FSW have not been measured experimentally. However, several modeling techniques have been used to estimate the strain rates during FSW of Al alloys including a kinematic approach [26], CTH or "hydrocode" [27], computational fluid dynamics (CFD) models [16, 17], solid-mechanics model [14, 15] and a formalism using the Zener-Holloman parameter [28, 29]. Maximum strain rates ranging from 10^1 to 10^3 s^{-1} have been reported with the consensus of estimates falling between 10^2 and 10^3 s^{-1}.

While the strain and strain rates experienced in the welds made in this study are not accurately known, the presence of banding can still be rationalized based on the trends regarding the local variation of strains and strain rates across the weld as explained by Seidel and coworkers [16, 17]. Banding on advancing side for both welds appeared to result from the greater strains and strain rates experienced by the material originating on the advancing side that is carried around the retreating side and finally

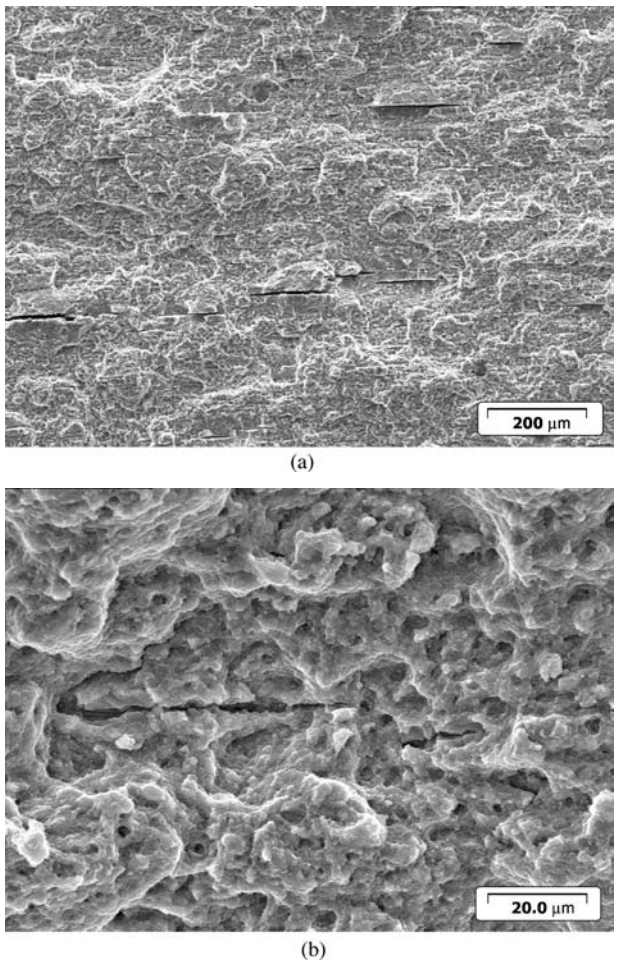

Figure 11 SEM fractographs of tensile specimen in AA-8009 base metal.

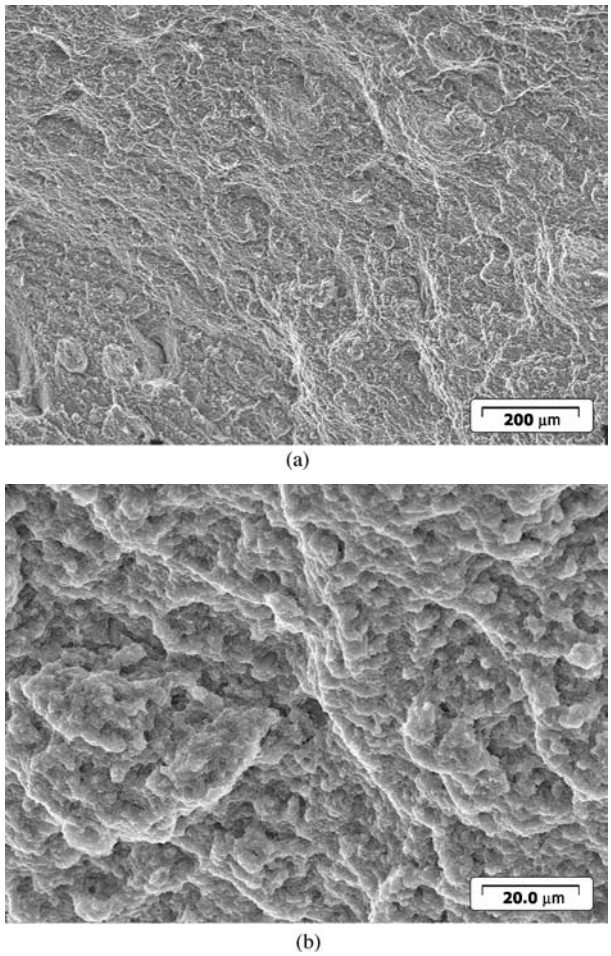

Figure 12 SEM fractographs of tensile specimen in FSW AA-8009 at a tool rotational speed of 1200 rpm and a traversing rate of 4.3 mm/s.

deposited on the advancing side, see Fig. 1 [16, 17]. Material starting (and finishing) on the retreating side apparently did not experience strains and strain rates sufficient to cause banding. The more extensive banding found in Weld 1 may be attributed to the greater strain rates associated with the higher rotational speed used.

The sharp interface observed on the advancing side of both welds delineates the locus of positions where the streamlines from the advancing and retreating side converged and rejoined behind the pin. The presence of defects along this sharp interface in Weld 1 resulted from incomplete bonding of the material from the two converging fronts due improper welding conditions, apparently related to excessive rotational speed for that weld.

As discussed previously, deformation-induced bands have been observed at the outer periphery of inertia-friction welds in this and similar dispersoid-strengthened aluminum alloys [20–24], at weld locations where the temperature is highest and deformation strains are the most severe. Some debate exists regarding the formation mechanism of the dispersoid-lean regions. It has been suggested that at these locations, the combined shear and compressive stresses may locally extrude soft alpha aluminum matrix containing a low dispersoid population from the original base metal microstructure [20, 21]. This mechanism may also explain the presence of both high-population and low-population dispersoid regions, although in the FSW welds the low-dispersoid regions were much more apparent. Considering the high temperatures and intense deformation experienced in the FSW pin region, it is likely that a similar mechanism may have promoted the formation of these banded regions. A significant reduction in banding and appreciably less difference in dispersoid population density between banded and surrounding regions were observed for Weld 2, which was produced at a lower tool rotational speed and lower traversing rate. This observation is consistent with the comparatively lower deformation rates experienced in this weld versus Weld 1 and is corroborated by similar trends with RPM in inertia-friction welds on the same material. It is expected that further optimization of welding parameters, including tool design, would further reduce stir-zone microstructural heterogeneities.

The observed improvement of weld zone tensile strength for Weld 2 is consistent with its improved weld zone microstructural homogeneity and absence of defects at the weld zone/base metal boundary. It is anticipated that

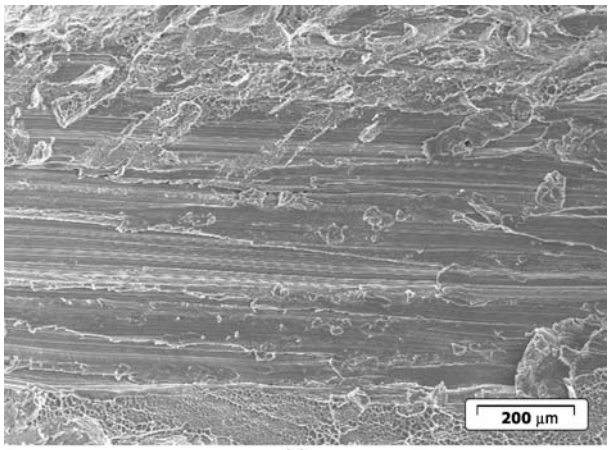

(a)

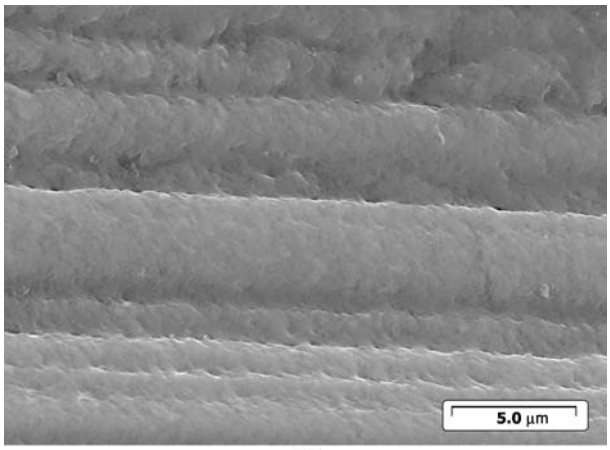

(b)

Figure 13 SEM fractographs of tensile specimen in FSW AA-8009 at tool rotational speed of 1200 rpm and a traversing rate of 4.3 mm/s. Note smooth, featureless fracture surface located at advancing weld side boundary.

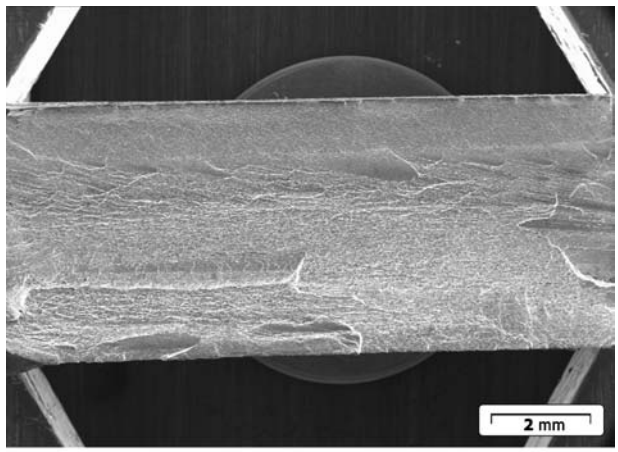

(a)

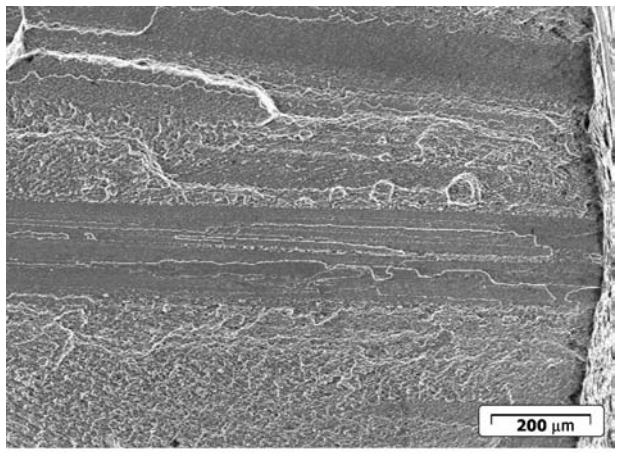

(b)

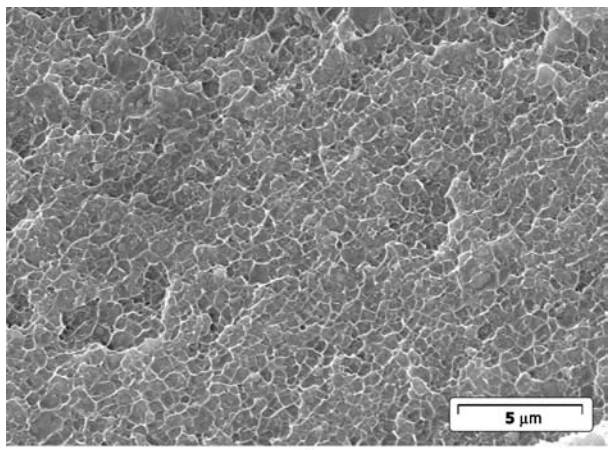

(c)

Figure 14 SEM fractographs of tensile specimen in FSW AA-8009 at a tool rotational speed of 428 rpm and traversing rate of 1.9 mm/s: (a) low magnification; (b) surface region showing smooth fracture; (c) region of smooth fracture at increased magnification.

further homogenization would increase strength to nearly 100% joint efficiency.

Many of the features of the welds produced in this study are consistent with and corroborate those observed by Reynolds and coworkers [8–10] as well as Murr and coworkers [2–6]. These features include evidence of backward flow on the retreating side and forward flow on the advancing side of Weld 1 in accord with results reported by Reynolds and coworkers [8–10]. The bulge on advancing side of the stir zone is another interesting feature. Similar bulges have been reported in FSWs by other researchers when the pin diameter is large [9], although other welding conditions may also cause bulges. The cause of the bulge in the present work is not clear. It may have developed due to flow around advancing side at excessive rotational speed. The complex, repetitive flow features shown in the various sections of this study also bear similarities to those reported by Murr and coworkers [2–6].

It is important to note that the variations in contrast and hardness seen here differ in origin from those seen by Murr and coworkers, despite the similarity in complicated and repeating patterns observed in the two efforts. The studies by Murr and coworkers involved dissimilar-alloy welds between aluminum and copper or between different aluminum alloys. Contrast and hardness variations in their work resulted from intermixing of dissimilar alloys with different etching behaviors and different mechanical properties after welding. These effects would not be observed in single alloy welds (i.e. not dissimilar) with

the same set of alloys. One of the drawbacks to studying flow patterns in FSWs between dissimilar Al alloys and between Al and Cu alloys relates to the differences in flow stress at welding temperatures. These differences may give rise to flow patterns that are not representative of same alloys welds that in turn cause the large volumetric defects seen in many of the dissimilar welds.

The current work employed a single, initially homogeneous material produced by very different processing than the alloys used by Murr and coworkers and with a very different microstructure. The variations in contrast and hardness stemmed from the development of dispersoid-lean bands that resulted from the high strain rate deformation experienced during FSW. They apparently delineate regions that have experienced high strain rates and could be observed on unetched metallographic samples. Moreover, aside from the small defects seen in Weld 1, the welds produced in this study were free from large volumetric defects common to dissimilar welds. The current work eliminates concerns with the effects of differences in flow stress on the formation of the intercalated flow patterns in dissimilar alloy FSWs and provides evidence that repetitive flow patterns can form in a single monolithic material.

An important consequence of this work relates to the use of friction-stir processing (FSP) to homogenize the distribution of dispersoids in advanced aluminum alloys, including alloys similar those evaluated in the present study [30]. As has been demonstrated in such FSP work, the use of optimized parameters can promote desired microstructural homogenization. However, this process has the potential to promote macrostructural heterogeneities in the form of bands of nearly dispersoid-free regions. The size and continuous nature of these very soft regions could lead to a reduction in material properties. Therefore, it is critical that FSP parameters be fully optimized in order to preclude such effects.

4. Conclusions

1. Results of the present study have shown that the control of friction stir welding process parameters (use of a lower tool rotational speed and lower traversing rate) can result in the production of high-integrity welds in dispersion-strengthened, elevated-temperature AA-8009.

2. Intense, non-uniform high temperature deformation along the advancing side weld interface during welding at a tool rotational speed of 1200 rpm and a traversing rate of 4.3 mm/s promoted the presence of lack-of-bonding defects. In addition, macroscopically heterogenous dispersoid structures were formed on the advancing side of the weld zone, with distinct bands of dispersoid-lean and dispersoid-enriched regions. A lower tool rotational speed of 428 rpm and lower traversing rate or 1.9 mm/s reduced the extent of these regions and promoted a more uniform dispersoid distribution across the weld zone.

3. The dispersoid-lean bands apparently formed in regions of highest strain and strain rate during FSW. They may have formed due to some type of shear banding, possibly adiabatic shear banding. Consequently, the 8009 alloy may be useful for studying the relation between process parameters and local strain and strain rate during FSW.

4. Hardness across the weld zones was slightly lower than that of the unaffected base metal, except in banded regions of low dispersoid density, which exhibited appreciable softening. The elimination of defects and dispersoid-lean, low hardness regions in the low tool rotational speed and traversing rate weld promoted an increase in joint efficiency from 77 to 89%. Weld specimen ductilities remained well below that of the base metal, in part due to strain localization in the lower strength weld zone region of the transverse-weld oriented test specimens.

5. Fracture of the transverse-weld oriented tensile specimens occurred exclusively near the boundary between the weld zone and the base metal on the advancing side of the weld. Fracture surfaces for the base metal and weld metals typically exhibited microvoids that nucleated at fine dispersoid particles, and tear ridges. Weld 1 specimens fractured along the base metal/weld zone interface on the advancing side of the weld, and exhibited occasional, smooth, featureless features that suggested incomplete bonding along this interface. Fracture of Weld 2 specimens also occurred near the base metal/weld zone interface, but did not exhibit such featureless surfaces, which is consistent with their superior mechanical properties.

Acknowledgments

The authors express appreciation to Allied-Signal, Inc., for providing the alloy evaluated in this study. Thanks are also extended to Mr. W.L. Stellwag, Jr. and The Edison Welding Institute for producing the welds examined in this investigation. Finally, the authors would like to acknowledge Ms. Jill Evans of Rensselaer Polytechnic Institute for her graphics contributions. Work performed by W. A. Baeslack III on this program was in his capacity as a reserve officer in the U.S. Air Force

References

1. T. J. LIENERT, R. J. GRYLLS, J. E. GOULD and H. L. FRASER, in "Proceedings of TMS Symposium on Hot Deformation in Aluminum Alloys I," edited by T. R. Bieler, L. A. Lalli and S. R. MacEwen (TMS, 1998) 159.
2. L. E. MURR, R. D. FLORES, O. V. FLORES, J. C. MCCLURE, G. LIU and D. BROWN, *Mat. Res Innovat.* **1** (1998) 211.
3. L. E. MURR, Y. LI, R. D. FLORES, E. A. TRILLO and J. C. MCCLURE, *ibid.* **2** (1998) 150.
4. Y. LI, L. E. MURR and J. C. MCCLURE, *Mat. Sci. and Eng.* **A271** (1999) 213.
5. Y. LI, L. E. MURR and J. C. MCCLURE, *Scripta Mat.* **40** (1999) 1041.
6. S. H. KAZI and L. E. MURR, in "Proceedings of Symposium on Friction Stir Welding and Processing," edited by K. V. Jata, M. W. Mahoney, R. S. Mishra, S. L. Semiatin and D. P. Field (TMS, 2002) 139.

7. K. COLLIGAN, *Weld. J., Res. Suppl.* **78** (1999) 229s.
8. A. P. REYNOLDS, T. U. SEIDEL and M. SIMONSEN, in Proceedings of the 1st International Symposium on Friction Stir Welding, edited by P. Threadgill (TWI, 1999) Session 4, Paper 1.
9. A. P. REYNOLDS, *Sci. and Tech. of Weld. and Join.* **5**(2) (2000) 120.
10. T. U. SEIDEL and A. P. REYNOLDS, *Met. and Mat. Trans. A,* **32A** (2001) 2879.
11. M. GUERRA, J. C. MCCLURE, L. E. MURR and A. C. NUNES, in "Proceedings of Symposium on Friction Stir Welding and Processing," edited by K. V. Jata, M. W. Mahoney, R. S. Mishra, S. L. Semiatin and D. P. Field (TMS, 2002) 25.
12. B. LONDON, M. W. MAHONEY, W. BINGEL, M. CALABRESE, R. H. BOSSI and D. WALDRON, in "Proceedings of Symposium on Friction Stir Welding and Processing II," edited by K. V. Jata, M. W. Mahoney, R. S. Mishra, S. L. Semiatin and T.J. Lienert (TMS, 2003) 3.
13. G. J. BENDZSAK, T. H. NORTH and C. B. SMITH, in "Proceedings of the 2nd International Symposium on Friction Stir Welding," edited by P. Threadgill (TWI, 2000) Session 4, Paper 1.
14. S. XU, X. DENG, A. P. REYNOLDS and T. U. SEIDEL, *Sci. and Tech. of Weld. and Join.* **6**(3) (2001) 191.
15. X. DENG and S. XU, *Transactions of NAMRI/SME.* XXIX (2001) 631.
16. T. U. SEIDEL and A. P. REYNOLDS, *Sci. and Tech. of Weld. and Join.* **8**(3) (2003) 175.
17. T. U. SEIDEL, Ph.D. Dissertation, (Department of Mechanical Engineering, University of South Carolina, 2001) p. 155.
18. High Temperature Aluminum Alloy 8009 Data Sheet (Allied Signal Inc., Morristown, NJ).
19. D. J. SKINNER, in "Dispersion Strengthened Aluminum Alloys" edited by Y. W. Kim and W. M. Griffith, (TMS/AIME, Warrendale, PA, 1988) pp. 181.
20. H. KOO, S. KRISHNASWAMY and W. A. BAESLACK III, *Mat. Char.* **26** (1991) 123.
21. H. KOO and W. A. BAESLACK III, *Weld. J. Res. Suppl.* **71** (1992) 147s.
22. T. J. LIENERT, W. A. BAESLACK III, J. RINGNALDA and H. L. FRASER, *J. Mat. Sci.* **31** (1996) 2149.
23. T. J. LIENERT, J. M. K. WIEZOREK, H. L. FRASER and W. A. BAESLACK III, in "Proceedings of Joining of Advanced and Specialty Materials," edited by M. Singh, J. E. Indacochea and D. Hauser (ASM, 1998) 107.
24. T. J. LIENERT, P. B. NAGY and W. A. BAESLACK III, *Weld. J., Res. Suppl.* **77** (1998) 14s.
25. S. P. TIMOTHY, *Acta Metall.* **35** (1987) 301.
26. A. C. NUNES, JR, in Proceedings of the TMS Annual Meeting Aluminum Automotive and Joining Symposia, edited by S. K. Das, J. G. Kaufman and T. J. Lienert (TMS, 2001) pp. 235.
27. A. ASKARI, S. SILLING, B. LONDON and M. W. MAHONEY, in "Proceedings of Friction Stir Welding and Processing," edited by K. V. Jata, M. W. Mahoney, R. S. Mishra, S. L. Semiatin and D. P. Field (TMS, 2001) pp. 43.
28. O. T. MIDLING and Ø. GRONG, *Acta Metall. et Mater.* **42** (1994) 1595.
29. Ø. FRIGAARD, Ø. GRONG, J. HJELEN, S. GULBRANDSEN-DAHL and O. T. MIDLING, in "Proceedings from the 1st International Friction Stir Welding Symposium," edited by P. Threadgill (TWI, 1999), Session 11, Paper B.
30. J. ZHENG, R. S. MISHRA, P. BERBON and M. W. MAHONEY, in "Proceedings of Symposium on Friction Stir Welding and Processing," edited by K. V. Jata, M. W. Mahoney, R. S. Mishra, S. L. Semiatin and D. P. Field (TMS, 2002) pp. 235.

Received 9 January
and accepted 7 July 2005